Isoform- and Phosphorylation-specific Multiplexed Quantitative Pharmacodynamics of Drugs Targeting PI3K and MAPK Signaling in Xenograft Models and Clinical Biopsies 🅐🅒

William G. Herrick[1], Casey L. Kilpatrick[1], Melinda G. Hollingshead[2], Dominic Esposito[3], Geraldine O'Sullivan Coyne[4], Andrea M. Gross[5,6], Barry C. Johnson[4], Alice P. Chen[4], Brigitte C. Widemann[5,6], James H. Doroshow[4,6], Ralph E. Parchment[1], and Apurva K. Srivastava[1]

ABSTRACT

Ras/Raf/MEK/ERK (MAPK) and PI3K/AKT signaling pathways influence several cell functions involved in oncogenesis, making them attractive drug targets. We describe a novel multiplex immunoassay to quantitate isoform-specific phosphorylation of proteins in the PI3K/AKT and MAPK pathways as a tool to assess pharmacodynamic changes. Isoform-specific assays measuring total protein and site-specific phosphorylation levels of ERK1/2, MEK1/2, AKT1/2/3, and rpS6 were developed on the Luminex platform with validated antibody reagents. The multiplex assay demonstrated satisfactory analytic performance. Fit-for-purpose validation was performed with xenograft models treated with selected agents. In PC3 and HCC70 xenograft tumors, the PI3Kβ inhibitor AZD8186 suppressed phosphorylation of AKT1, AKT2, and rpS6 for 4 to 7 hours post single dose, but levels returned to baseline by 24 hours. AKT3 phosphorylation was suppressed in PC3 xenografts at all doses tested, but only at the highest dose in HCC70. The AKT inhibitor MK-2206 reduced AKT1/2/3 phosphorylation in SW620 xenograft tumors 2 to 4 hours postdose, and the MEK inhibitor selumetinib reduced MEK1/2 and ERK1/2 phosphorylation by up to 50% and >90%, respectively. Clinical utility was demonstrated by analyzing biopsies from untreated patients with plexiform neurofibromas enrolled in a clinical trial of selumetinib (NCT02407405). These biopsies showed MEK and ERK phosphorylation levels sufficient for measuring up to 90% inhibition, and low AKT and rpS6 phosphorylation. This validated multiplex immunoassay demonstrates the degree and duration of phosphorylation modulation for three distinct classes of drugs targeting the PI3K/AKT and MAPK pathways.

Introduction

Constitutively high pathway expression via ligand–receptor interactions or somatic mutations to key enzymes in the Ras/Raf/MEK/ERK (MAPK) or PI3K/AKT pathways drive or sustain many types of cancer (1, 2). Multiple pathways drive complex signaling interactions that make it difficult to inhibit the growth of tumor cells; inhibition at any one point in a pathway can be overcome by mutation, altered expression of other pathway components, or use of alternative isoforms or splice variants (3, 4).

Signaling pathway inhibitors often have multiple physiologic effects that limit clinical utility. For example, pan-PI3K inhibitors disrupt signaling leading to tumor growth, but can also cause metabolic changes leading to severe hyperglycemia (5, 6). Drug development is also complicated by rapid development of resistance via altered expression and activation of factors within the targeted pathway. Isoform-specific inhibition of PI3Kα or PI3Kβ activity can be overcome by mutations in downstream components in the pathway (7) or compensatory expression of off-target isoforms (8). Monitoring downstream target status is critical for drug development as feedback reactivation has been observed in multiple studies of compounds targeting the PI3K/AKT/MAPK pathway (9–11). The cooperative nature of signaling pathways is demonstrated by recent descriptions of non–small cell lung cancer (NSCLC)–derived cell lines resistant to gefitinib despite the fact that the drug caused inhibition of its intended target (12) and of breast cancer cells treated with PI3K or AKT inhibitors that experienced an increase in SGK3 expression and subsequent activation of the mTORC1 pathway (13). Despite these obstacles, there are promising compounds with demonstrated activity in the form of prolonged progression-free and overall survival against mutated tumors (14).

Developing more effective inhibitors of cell signaling pathways requires detailed information about the drug's effects on multiple points within the pathway. Pharmacodynamic analyses using more traditional methods (e.g., Western blotting, immunohistochemistry) are limited for several reasons (15). First, clinical benefits can occur when phosphorylation of a target protein is inhibited, even if the

absolute protein concentration remains unaffected (16). The techniques themselves are labor-intensive and low-throughput, have poor signal-to-noise ratios, and data resulting from these techniques are difficult to quantitate. These techniques are also limited in the number of analytes that can be quantified in a given sample. This study describes a multiplex immunoassay that overcomes these limitations to measure key pharmacodynamic changes to the MAPK and PI3K/AKT pathways. The broad analysis of pharmacodynamic effects possible with this multiplex assay offers benefits and eliminates several obstacles that complicate more traditional methods. Importantly, it allows for simultaneous evaluation of multiple points along a signaling pathway in addition to phosphorylation of proteins in an untargeted pathway. The immunoassays are isoform-specific to MEK1/2, ERK1/2, and AKT1/2/3, as recent discoveries elucidated isoform-specific roles in normal tissues and cancer physiology (17–21). Measuring levels of PI3K protein expression in a multiplex assay is difficult due to the number of isoforms and mutations (22). Also, unlike AKT, MEK, and ERK, PI3K activity is not directly linked with phosphorylation status. Therefore, PI3K was not selected for inclusion in these assays. The immunoassays also include ribosomal protein S6 (rpS6) as an indicator of downstream activation that may arise from alternative signaling pathways, as rpS6 is differentially phosphorylated by both the MAPK and PI3K/AKT pathways (23). The capture antibodies described here are specific to individual isoforms of the respective proteins, allowing for more detailed analysis of drug responses. The assay can be performed with tissue from a single needle core biopsy and performed in a more reproducible manner than with some other techniques (15).

We measured these readouts at multiple time points in xenograft model experiments to provide a detailed analysis of the magnitude and duration of inhibition for each of the agents. Such analyses can be used to guide dosages and dosing schedules in future studies (24). In addition, identifying alternative pathways activated in response to a targeted treatment may inform the selection of effective treatment combinations to counter the development of resistance via cross-pathway activation. This multiplex assay therefore offers a validated approach to quantitatively assess pharmacodynamic responses at multiple points within and across signaling pathways simultaneously.

Materials and Methods
Antibodies and recombinant protein calibrators
Recombinant calibrator proteins were purchased or purified as fusion proteins with at least one affinity tag, either glutathione S-transferase (GST), polyhistidine (6His), or maltose-binding protein (MBP). Manufacturers are specified in the Supplementary Methods. Purity was assessed by SDS-PAGE and protein concentrations measured by the Bradford method (Bio-Rad) with BSA as a calibrator (Thermo Fisher Scientific). Detection antibodies were conjugated to biotin using Sulfo-NHS-LC-Biotin (Thermo Fisher Scientific) and excess biotin was removed with Zeba Spin Desalting columns (Thermo Fisher Scientific).

Xenograft studies
All animal studies were conducted in accordance with an approved animal care and use committee protocol accredited by the Association for Assessment and Accreditation of Laboratory Animal Care International and follows the USPHS Policy for the Care and Use of Laboratory Animals. Female athymic nude mice (nu/nu NCr, 5–6 weeks old; Biological Testing Branch, NCI, Frederick, MD) were implanted with HCC70 (human breast carcinoma) and male athymic nude mice (8–12 weeks old) were implanted with PC3 (human prostate

cancer) or SW620 (human colorectal adenocarcinoma) cell lines by subcutaneous injection as described previously (25). Each cell line was authenticated by analyzing short tandem repeat DNA screening using AmpFLSTR Identifier (Applied Biosystems) and was passaged no more than 20 times. All experimental therapeutic agents (AZD8186, MK-2206, and selumetinib) were obtained from the Division of Cancer Treatment and Diagnosis (DCTD) Investigational Drug Repository. AZD8186 (NSC 777572; ref. 26) was administered orally in vehicle [10% DMSO, 60% triethylene glycol (or PEG300), and 30% water]. MK-2206 (NSC 756656; ref. 27) and selumetinib (ARRY-142886, NSC 741078) were administered as single agents or as a two-drug regimen in vehicle (0.5% hydroxypropyl methylcellulose and 0.1% polysorbate buffer).

Mice were randomized into treatment arms when tumors reached 200 ± 25 mm^3. Mice bearing PC3 or HCC70 xenografts were dosed with vehicle, 25 or 50 mg/kg AZD8186 either once ("single dose") or every 12 hours for 1 week ("multiple dose") with vehicle or with 50 mg/kg AZD8186. Tumors were collected 2, 4, 7, and 24 hours after administration in the single-dose groups or 4 (HCC70), 7 (PC3), 12, and 24 hours post final dose ($n = 4$ mice per group) in multidose groups. Mice bearing SW620 xenografts were dosed with vehicle, 24 mg/kg MK-2206 alone, 20 mg/kg selumetinib alone, or MK-2206 and selumetinib in combination either once ("single dose") or for three weeks with weekly MK-2206 and/or daily selumetinib ("multiple dose": MK-2206 every 7 days for four doses on days 1, 8, 15, and 22; selumetinib every day for 21 days on days 1–21). Tumors were collected 2, 4, 24, and 48 hours post final dose ($n = 5$ mice per group). All xenograft samples were flash-frozen with liquid nitrogen within 2 minutes of harvesting to preserve analytes (28).

Total protein extraction and denaturation
Samples were extracted as reported previously (28). A small portion of lysate was denatured for MEK/ERK assays as described in the Supplementary Methods. AKT/rpS6 immunoassays did not require denaturation and remaining aliquots not denatured for MEK/ERK analysis were flash-frozen after extraction.

Luminex multiplex immunoassays
All multiplexed immunoassays were developed on the Luminex xMAP technology platform using MagPlex polystyrene-coated magnetic beads (Luminex) and performed in flat-bottomed black 96-well plates (Bio-Rad) protected from light with black microplate lids (VWR) during all incubations. Buffer ingredients are listed in the Supplementary Methods. Lysates were diluted to 125 µg/mL in Capture Buffer, loaded on plates at 40 µL/well, and MagPlex bead cocktails were loaded at 10 µL/well. Plates were incubated for 2 hours at room temperature ($20 \pm 3°$C) with shaking at 850 rpm for AKT/rpS6 or at $4 \pm 3°$C overnight (16–18 hours) for MEK/ERK. All subsequent incubations were performed at room temperature. Plates were then washed three times using a BioTek 405 TS plate washer with 300 µL/well/wash of AKT/rpS6 wash buffer or MEK/ERK wash buffer. After washing, 50 µL/well of antibody–biotin conjugate in detection buffer was added and the plates were incubated with shaking for 1 hour. Plates were washed again as described above. Premium grade R-phycoerythrin–labeled streptavidin (Invitrogen, 50 µL/well) was added and the plates were incubated with shaking for 30 minutes. Plates were washed again as described above, and then the beads were resuspended in 100 µL/well of the appropriate wash buffer and incubated with shaking for 1 to 2 minutes. Plates were read on Luminex 200 readers with the High Photomultiplier Tube (PMT) setting. Data are presented in one of three ways: (i) picograms of analyte per

microgram of total protein for assay validation, (ii) the percent of phosphorylated analyte (phosphorylated/total analyte $\times$ 100) as percent of vehicle for xenograft experiments (rpS6 normalized using net median fluorescence intensity, or Net MFI, due to unstable phosphorylation of the recombinant calibrator), or (iii) the percent phosphorylation of the total analyte in the human biopsy samples.

Analytic validation

Control materials were generated from pooled lysates of xenografts and knockout cell line pellets spiked with recombinant proteins when necessary to achieve desired analyte concentrations. To ensure good analytic performance over a wide range of analyte concentrations, controls were optimized to have analyte concentrations at approximately the 20th and 80th percentiles of their respective standard curves. Assay precision was assessed by intraplate ($n = 20$) and interday ($n = 5$) measurements of the control materials. Dilutional linearity and dilutional recovery were assessed from six xenograft types (HT-29, MDA-MB-231T, U87MG, GTL16, PC3, and HCT116) and four sample dilutions. Accuracy was measured by spiking five or more xenograft types either with lysates having high endogenous analyte expression or recombinant calibrators and calculated as percent recovery. Intra- and intertumoral biological variability was measured in three models (HCC70, PC3, and SW620) as described previously (28).

Statistical analysis

Multiplex data were generated using Luminex xPONENT software. Standard curves were fitted using a 4- or 5-parameter logistic curve fit (Bio-Plex Manager v 6.1 or newer) for individual analytes. Fit-for-purpose preclinical model samples were analyzed by calculating the ratio (or percent) of phosphorylated to total analyte for every sample and then normalizing these values to the average vehicle sample value at each time point. To determine whether normalized analyte phosphorylation levels in the treatment groups were significantly different from corresponding vehicle phosphorylation levels at each time point, we performed both Student t tests (unpaired, two-sided, assuming unequal variance; GraphPad Prism v8) and two-way ANOVA with follow-up (post hoc) tests for multiple comparisons (Supplementary Methods; Prism v8). The results of the two statistical hypothesis testing methods were largely in agreement (i.e., P values < 0.05), but some differed in the magnitude of significance; the disagreements between the methods are described in Supplementary Table S1. P values presented in the Results section are derived from Student t tests, as would be used to interpret data from clinical trials. Significant values are indicated in figures (*, $P < 0.05$; **, $P < 0.01$; ***, $P < 0.001$).

Patient selection and biopsy collection

Patients with neurofibromatosis type 1 (NF1) and inoperable plexiform neurofibromas (PNs) were enrolled in a phase II clinical trial assessing the efficacy of selumetinib (NCT02407405). This study enrolled patients with a documented germline NF1 mutation (29) in the neurofibromatosis type 1 gene performed in a Clinical Laboratory Improvement Amendments (CLIA)-certified laboratory or a diagnosis of NF1 based in clinical NIH consensus criteria (30, 31) of at least one other diagnostic criterion in addition to the presence of a PN. The study includes prospective evaluation of serial PN and cutaneous neurofibroma (cNF) biopsies. All patients gave written informed consent for study participation. Study design and conduct complied with all applicable regulations, guidances, and local policies, and the studies were approved by the NCI Institutional Review Board.

Baseline 18-gauge needle biopsies were collected from tumor tissues of patients with neurofibromas before the start of treatment with selumetinib. Biopsy cores were placed individually in prechilled cryogenic vials, frozen within 2 minutes of collection, stored at $\leq$ $-80°$C until extractions were performed as described previously (28), and processed according to Standard Operating Procedures (SOP) 340507 and 341201 published on the NCI/DCTD website (http://dctd. cancer.gov/ResearchResources/ResearchResources-biomarkers.htm).

Results

### Assay development and analytic validation

Antibody isoform specificity was validated via Western blot analysis with knock-out cell lines (Supplementary Fig. S1). Phosphorylation site specificity was validated using drug-treated cancer cell lines and peptide competition (Supplementary Fig. S2). An rpS6 antibody and isoform-specific antibodies to ERK1, ERK2, MEK1, MEK2, AKT1, AKT2, and AKT3 were selected as capture reagents for the respective analytes and biotinylated antibodies to pan-isoform total or phosphorylation site-specific epitopes were used for detection reagents (**Fig. 1A**).

The multiplex assays were grouped into five panels: two MEK/ERK panels (total analyte and phosphorylated analyte; **Fig. 1B**) and three AKT/rpS6 panels (one panel of total analyte and two panels of phosphorylated analyte, referred to as the phospho A and phospho B panels; **Fig. 1C**). The isoform specificities of antibodies in each panel were evaluated via multiplex immunoassays using isoform-specific knockout cell lines (Supplementary Table S2); the AKT knockout cell lines are derived from the DLD-1 cell line that does not express AKT3 (32), and basal phosphorylation of AKT is low. To highlight isoform specificity, phosphorylation was pharmacologically enhanced with the ATP-competitive AKT inhibitor, AZD5363 (33).

Typical calibrator curves for each assay are shown in **Fig. 1B** and **C**. Analytic validation of the assays was performed with results presented in Supplementary Table S3. Inter-assay precision is < 12% CV for AKT/rpS6 assays and < 24% CV for all MEK/ERK assays except phospho-ERK2 (26.9% CV); intra-assay precision is $\leq$ 13% CV for all analytes. Dilutional linearity and recovery were observed with lysates from several xenograft types, with all R^2 values greater than 0.97 and mean recoveries of 92 to 109% (data from dilutional linearity at 31.25 µg/mL sample concentrations were poor for some AKT/rpS6 analytes and are excluded). Spike recovery experiments were performed with calibrators in several xenograft types and ranged from 90% to 114% for all AKT isoforms and 78% for total rpS6. Spike recovery experiments performed with recombinant proteins were low (48% to 60%) for total ERK2, phospho-MEK1, and phospho-ERK1/2, but ranged from 84% to 99% when evaluated with endogenous protein spiking. Overall, the analytic performance of the assays is acceptable for analyzing batched samples. Surrogate intra- and inter-tumor biological variability, defined as least significant change (28), was model-dependent (Supplementary Table S2) with the lowest overall variability in the HCC70 model.

Pharmacodynamics of AZD8186 in a PTEN-mutant breast cancer model

Time-, dose-, and isoform-dependent inhibition of AKT phosphorylation was determined in HCC70 xenografts treated with the PI3Kβ inhibitor AZD8186. AKT2 was the most abundant AKT isoform in vehicle-treated samples (52% of total AKT detected) while AKT1 and AKT3 were equally abundant, MEK1 was 12-fold more abundant than MEK2, and ERK1/2 were present in approximately a 2:1 proportion.
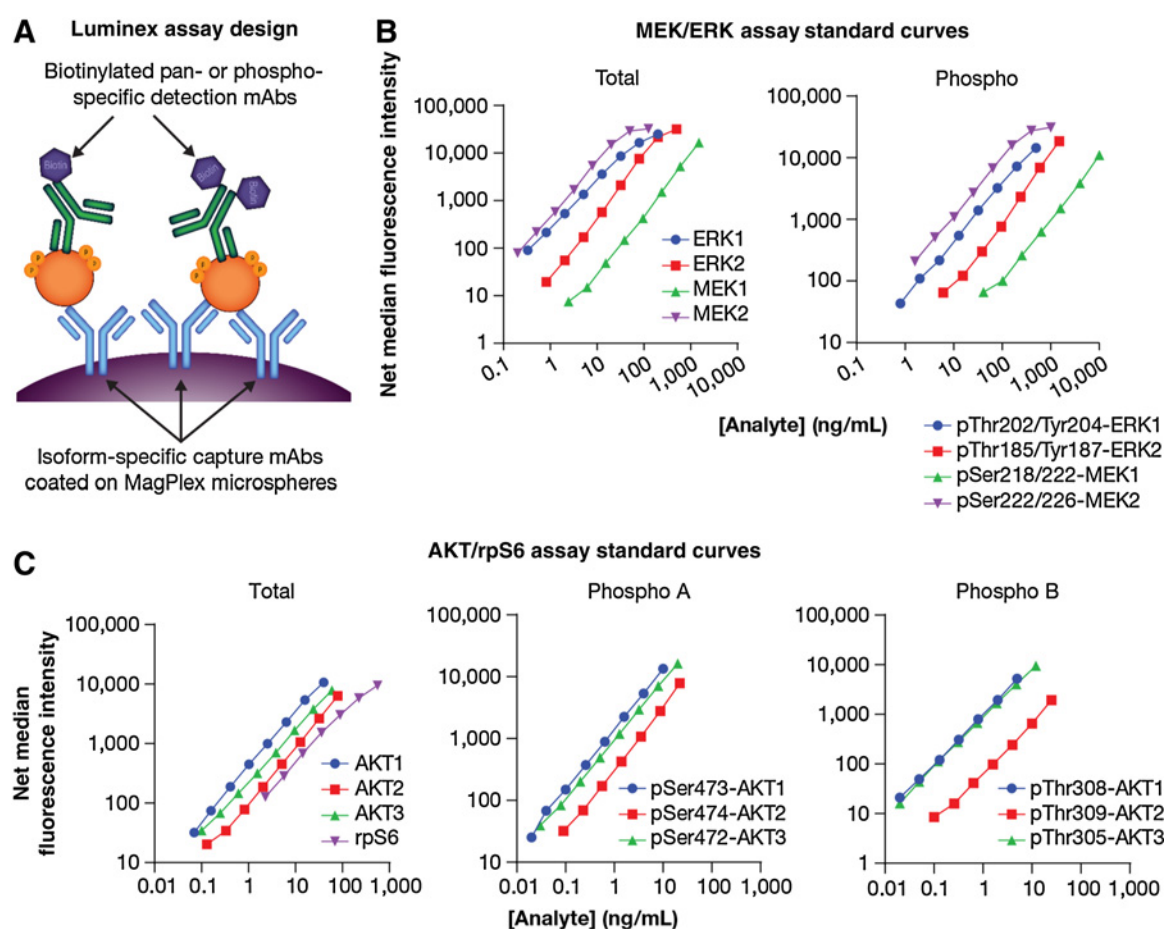
Figure 1.
Overview of Luminex multiplex assay. **A,** Quantitative isoform-specific Luminex sandwich immunoassays were developed with isoform-specific mAbs conjugated to MagPlex microspheres and biotinylated pan-isoform mAbs for detection of total and site-specific phosphorylated protein. The assays are divided into five panels for validation: MEK/ERK Total, MEK/ERK Phospho, AKT/rpS6 Total, AKT/rpS6 Phospho A, and AKT/rpS6 Phospho B. Standard curves were fit for the MEK/ERK panels (**B**) and the AKT/rpS6 panels (total rpS6 only; **C**). Phosphorylation sites assayed in each phospho panel are indicated in the respective panels.

The absolute quantities and relative abundance of isoforms were comparable before and after AZD8186 dosing. Post single dose (psd), phosphorylation at both Thr308-AKT1 and Ser473-AKT1 was reduced by 80%–90% at either 25 mg/kg or 50 mg/kg, indicating PI3K/AKT1 pathway inhibition by AZD8186 (**Fig. 2A** and **B**). Both pThr309-AKT2 and pSer474-AKT2 were reduced in a dose-dependent manner, with 55% to 60% reduction in phosphorylation at both sites at 25 mg/kg and 75 to 80% reduction at 50 mg/kg. Phosphorylation levels of all sites in both AKT1 and AKT2 returned to near baseline levels by 24 hours psd, except for a statistically significant increase in phosphorylation at pSer473-AKT1 at 24 hours ($132 \pm 11\%$, $P = 0.017$) following a 50 mg/kg dose of AZD8186 (**Fig. 2B**). Phosphorylation at Thr305-AKT3 and Ser472-AKT3 was less affected by AZD8186 treatment (20% to 40% reductions, Supplementary Fig. S3). Phosphorylation of MEK and ERK isoforms was not inhibited to a statistically significant degree, but ERK1/2 phosphorylation increased to approximately 2-fold above baseline levels by 7 hours psd ($P = 0.0092$–0.040; **Fig. 2C** and **D**; Supplementary Fig. S3) before returning to near vehicle level by 24 hours psd. Phosphorylation of both Ser235-rpS6 and Ser240/244-rpS6 was inhibited by 50% to 60% at both 25 and 50 mg/kg at 2 hours psd

before returning to vehicle level by 7 hours psd (**Fig. 2E** and **F**). Total and phosphorylated protein levels were also measured following a course of 50 mg/kg AZD8186 given Q12H for 7 days ("multiple dose"), with times indicating the time from administration of the last dose to sample collection (post multiple dose, pmd). Phosphorylation at Thr308-AKT1, Ser473-AKT1, and Thr309-AKT2 was reduced by 60%–70% 4 hours pmd, but returned to vehicle levels by 12 hours pmd ($P = 0.00045$–0.022, Supplementary Fig. S4). Ser474-AKT2 phosphorylation was reduced by 40% at 4 hours pmd ($P = 0.0030$) before returning to baseline at 12 hours pmd. Both rpS6 sites showed elevated phosphorylation to 150% to 160% of vehicle values by 12 hours pmd, although large variation precluded statistical significance ($P = 0.15$–0.16).

Pharmacodynamics of AZD8186 in a PTEN-mutant prostate cancer model

Mice bearing PC3 xenografts were also treated with either 25 mg/kg or 50 mg/kg AZD8186. Relative proportions of AKT isoforms were comparable to HCC70 xenografts (59% AKT2, 19% AKT1, 22% AKT3). ERK2 was more abundant than ERK1 (59% ERK2) and MEK1 was approximately 7-fold more abundant than MEK2.
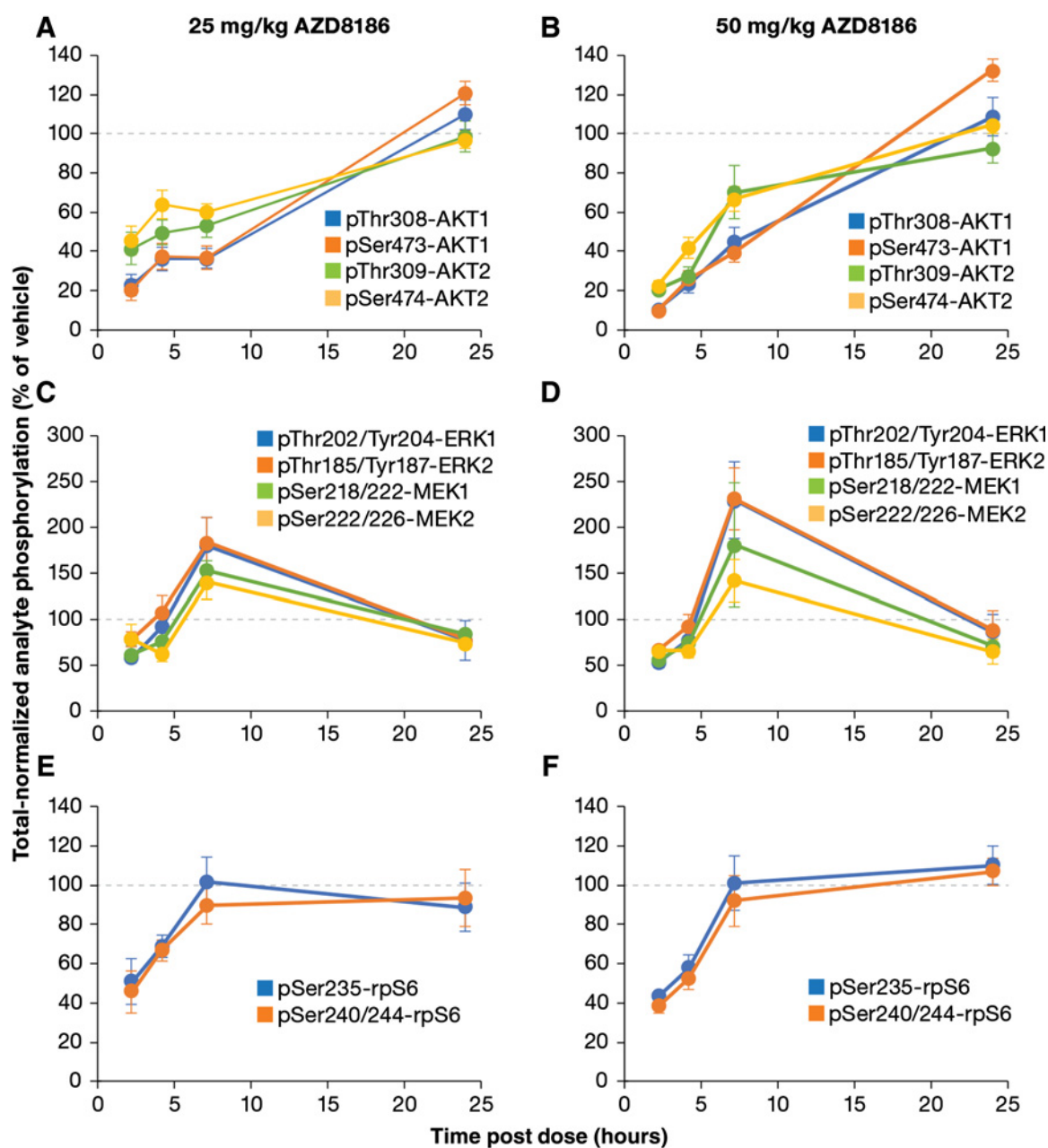
Figure 2.
Pharmacodynamic effects on selected PD endpoints in HCC70 xenografts following a single dose of AZD8186 ($n = 4$ mice/time point). Isoform-specific phosphorylation was measured relative to vehicle levels following doses of 25 mg/kg (**A, C,** and **E**) or 50 mg/kg (**B, D, F**). Data are presented as the mean of vehicle-normalized percent-phosphorylation at 2, 4, 7, and 24 hours psd. Error bars are SEM.

Phosphorylation of both sites on all AKT isoforms was inhibited by 50% to 80% at both dose levels 2 and 4 hours psd (**Fig. 3A–C**). Phosphorylation of Ser235-rpS6 was reduced 40% at 25 mg/kg 2 and 4 hours psd before returning to baseline levels by 7 hours psd. A single 50 mg/kg dose of AZD8186 reduced pSer240/244 by approximately 60% to 70% at 2 and 4 hours psd; statistically significant reduction of pSer240/244-rpS6 persisted to 7 hours psd with both 25 and 50 mg/kg doses ($P = 0.011$ for both doses; **Fig. 3D**; Supplementary Fig. S5). Both pSer235-rpS6 and pSer240/244-rpS6 returned to near vehicle phos-

phorylation levels at 24 hours psd. Following a 50 mg/kg dose, phosphorylation of ERK1/2 and MEK1/2 isoforms remained near vehicle levels, while MEK2 phosphorylation increased 24 hours psd at the lower dose ($158\pm22\%$, $P = 0.025$, Supplementary Fig. S5). Following a week-long course of 50 mg/kg AZD8186, phosphorylation at assayed sites of all AKT isoforms was reduced by 50% to 70%, although the change for pSer473-AKT1 was not statistically significant ($P = 0.065$, **Fig. 4**). Phosphorylation of all ERK and MEK isoforms peaked at 12 hours pmd with large distributions, but all returned to near vehicle
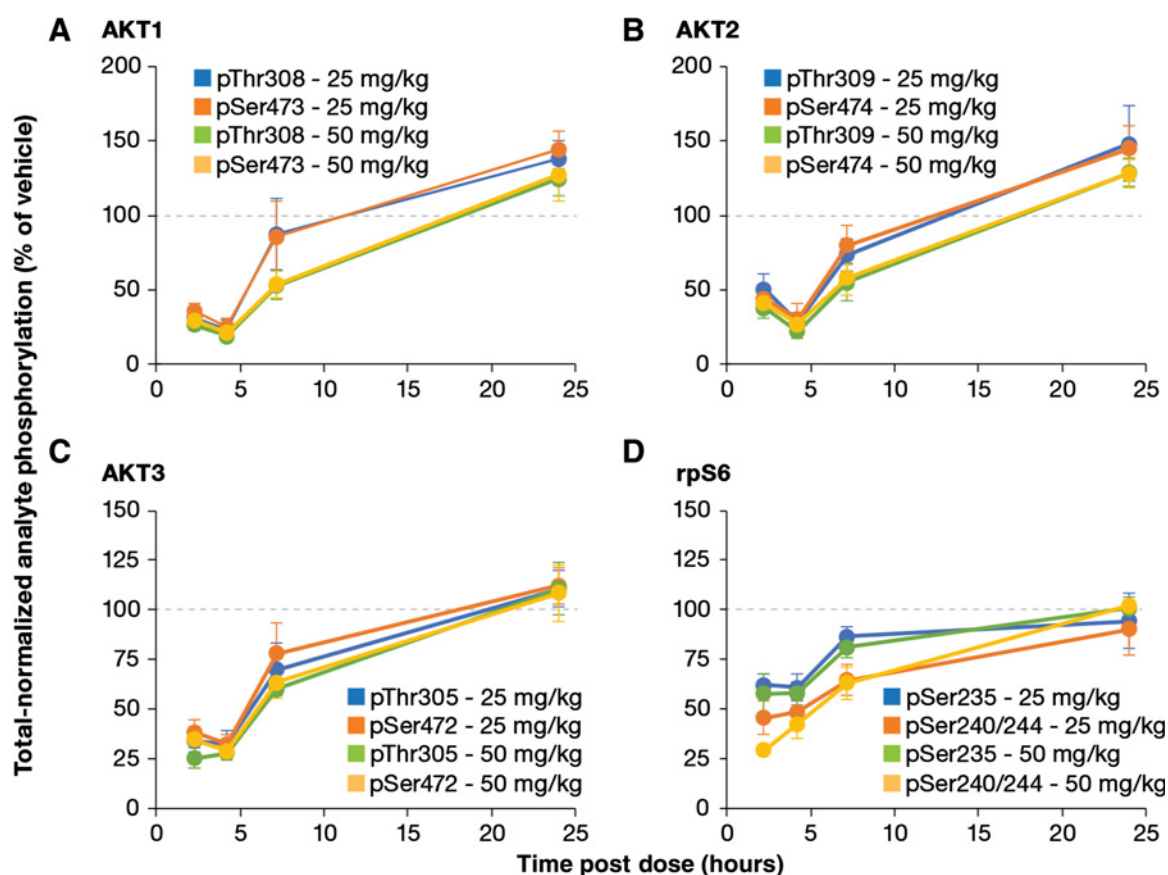
Figure 3.
Pharmacodynamic effects on phosphorylation of measured sites on AKT1 (**A**), AKT2 (**B**), AKT3 (**C**), and rpS6 (**D**) in PC3 xenografts following a single 25 mg/kg or 50 mg/kg dose of AZD8186 (*n* = 4 mice/time point). Data are presented as the mean of vehicle-normalized percent phosphorylation at 2, 4, 7, and 24 hours psd. Error bars, SEM.
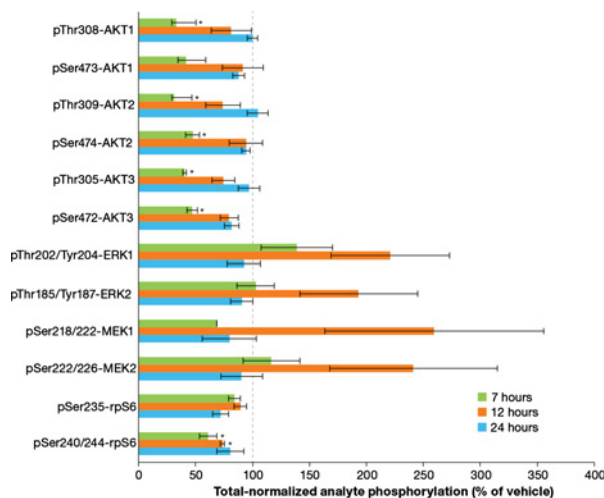

Figure 4.
Pharmacodynamic changes following the last dose of a week-long course of 50 mg/kg AZD8186 every 12 hours in PC3 xenograft-bearing mice (*n* = 4 mice/time point). Three time points post-last dose are shown for each analyte and are colored as indicated. Data are presented as the mean of vehicle-normalized percent phosphorylation. Error bars, SEM.

level at 24 hours pmd. Phosphorylation of Ser240/244-rpS6 was reduced by approximately 40% at 7 hours pmd and 25% at 12 hours pmd ($P = 0.033$ and 0.040, respectively); other values for the rpS6 sites were near vehicle levels (**Fig. 4**).

Pharmacodynamics of MK-2206 and selumetinib in a colon cancer model

Single doses of MK-2206 and selumetinib, non-ATP competitive allosteric inhibitors of AKT and MEK, respectively (34, 35), were given alone or in combination to mice bearing SW620 xenografts. AKT isoform proportions were comparable with the other xenograft types (57% AKT2, 26% AKT1, 18% AKT3), as were ERK isoforms (64% ERK2), and MEK1 was 17-fold more abundant than MEK2. MK-2206-treated samples showed 50% to 75% reductions in phosphorylation at both sites on all AKT isoforms at 2 hours psd, with the exception of pThr309-AKT2 ($P = 0.17$ for pThr309-AKT2, $P \le 0.0011$ for other AKT1/2/3 phosphorylation sites); phosphorylation returned to vehicle levels, or were elevated (pSer472-AKT3, $P = 0.048$), by 24 hours psd (Supplementary Fig. S6). Selumetinib potently decreased pThr202/Tyr204-ERK1 and pThr185/Tyr187-ERK2 (>90% reduction in phosphorylation, $P < 0.0002$ at 2 hours psd for both isoforms) at 2 and 4 hours psd; selumetinib decreased pSer218/222-MEK1 and pSer222/226-MEK2 to a lesser degree (40%–50% reductions, $P < 0.02$ for both
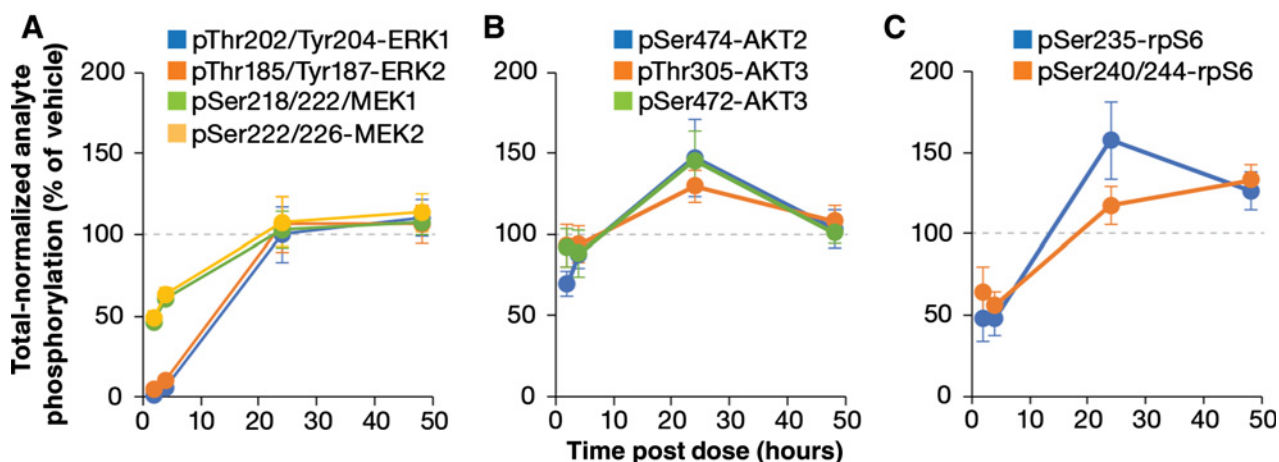
Figure 5.
Pharmacodynamic changes following a single 20 mg/kg dose of selumetinib in SW620 xenografts ($n = 5$ mice/time point). Data are presented as the mean of vehicle-normalized percent phosphorylation at 2, 4, 24, and 48 hours psd. (**A**, phospho-MEK/ERK; **B**, phospho-AKTs; **C** - phospho-rpS6) Error bars, SEM.

isoforms) at those time points (**Fig. 5A**). Interestingly, while ERK1/2 and MEK1/2 phosphorylation levels had returned to baseline by 24 hours psd, pThr305-AKT3 and pSer472-AKT3 were elevated to 130% to 150% of vehicle levels ($P = 0.044$ and 0.047, respectively), with corresponding elevated phosphorylation of pSer235-rpS6 ($P = 0.041$, **Fig. 5B** and **C**; Supplementary Fig. S6). No additional suppression of phosphorylation was quantified when the agents were given in combination; reductions of pThr309-AKT2 and pSer474-AKT2 at 4 hours psd could not be evaluated statistically as four of five samples were below the lower limit of quantitation (LLOQ, Supplementary Fig. S6). ERK1/2 and MEK1/2 phosphorylation levels were measured following a 3-week course of each single agent or the two agents together (Supplementary Fig. S7). Selumetinib again potently reduced pThr202/Tyr204-ERK1 and pThr185/Tyr187-ERK2 (>90% reduction of phosphorylation, $P < 0.00005$ for both isoforms), but pSer218/222-MEK1 and pSer222/226-MEK2 were elevated to approximately 140% to 165% of vehicle levels at 2 and 4 hours pmd ($P < 0.003$ for both isoforms) before returning to baseline by 24 hours pmd.

### Clinical fitness of pharmacodynamic assays

Eight unpaired, pretreatment 18-gauge needle core biopsies (one to three biopsies from each of four patients) and three cNF dermal shave biopsies (one biopsy each from three patients) were collected from patients with NF1-associated PNs enrolled on study to support assay validation. Biopsies were processed into total cell lysates as described previously (28) yielding total protein concentrations ranging from 660 to 4,172 µg/mL. The MEK/ERK immunoassays were able to measure baseline total protein levels and percent phosphorylation. Notably, the primary PD endpoints for selumetinib clinical trials, pERK1 and pERK2, were quantified in all samples and 10 of 11 samples, respectively (**Fig. 6**). Phosphorylated MEK1 was quantified in seven of 11 samples and pMEK2 was quantified in 10 of 11 samples. Total AKT1/2/3 levels were quantified in all but one (10 of 11) of the samples. Phosphorylated Ser473-AKT1 was low but quantifiable in three of 11 samples, and pSer474-AKT2 and pSer472-AKT3 were measurable in seven and eight of 11 samples, respectively. Phosphorylated rpS6 levels were very low in all samples; total rpS6 levels were measurable in four of

11 samples (**Fig. 6**). Ser474-AKT2 was the most highly phosphorylated site (mean = $50.2 \pm 32.5\%$ phosphorylation). ERK1/2 and MEK1 were the most abundant total analytes in both dermal and core biopsies (**Fig. 6A** and **B**). Percent phosphorylation was lower overall in the dermal biopsies than in the core biopsies (**Fig. 6C** and **D**), suggesting low basal PI3K/AKT pathway activity in these patient biopsies.

Discussion

The multiplex assay described here offers the ability to make quantitative, isoform-specific measurements of total and phosphorylated levels of analytes with protein extracted from a single core needle biopsy. This sample size advantage is notable, as core needle biopsies can involve significant risk and technical challenges (36). Care was taken to maximize the tumor content of biopsies and minimize dilution with normal tissue that may lead to erroneous conclusions (15). Preanalytic factors that may affect analyte stability must also be considered and minimized. Accordingly, stringent sample collection protocols have been applied to this study (28). Sample storage temperature and freeze–thaw stability, also critical for ensuring accurate and reliable assay results, have been evaluated and were acceptable for all of these assays. Nevertheless, to minimize the possibility of unforeseen issues in untested tissues, samples were initially assayed without prior freeze-thaw cycles, always kept cold, and processed as quickly as possible after thawing. Some MEK/ERK analytes showed poor recombinant protein spike recoveries. However, while MEK/ERK spike recoveries were poor for some analytes regardless of sample type, they were acceptable when lysates with high endogenous protein expression were used in place of recombinant protein calibrators. Assay analytic validation demonstrated acceptable overall performance and precision.

Measurement of phospho-AKT, -MEK, and -ERK have been described previously by various methodologies (37–39). However, assays developed in this study offer substantial advancement in terms of content and rigor of validation. The major distinctions are that our assays are isoform-specific, include all canonical isoforms of AKT, MEK, and ERK proteins, and measure phosphorylation sites in a sandwich format that improves specificity of phospho-antibodies,
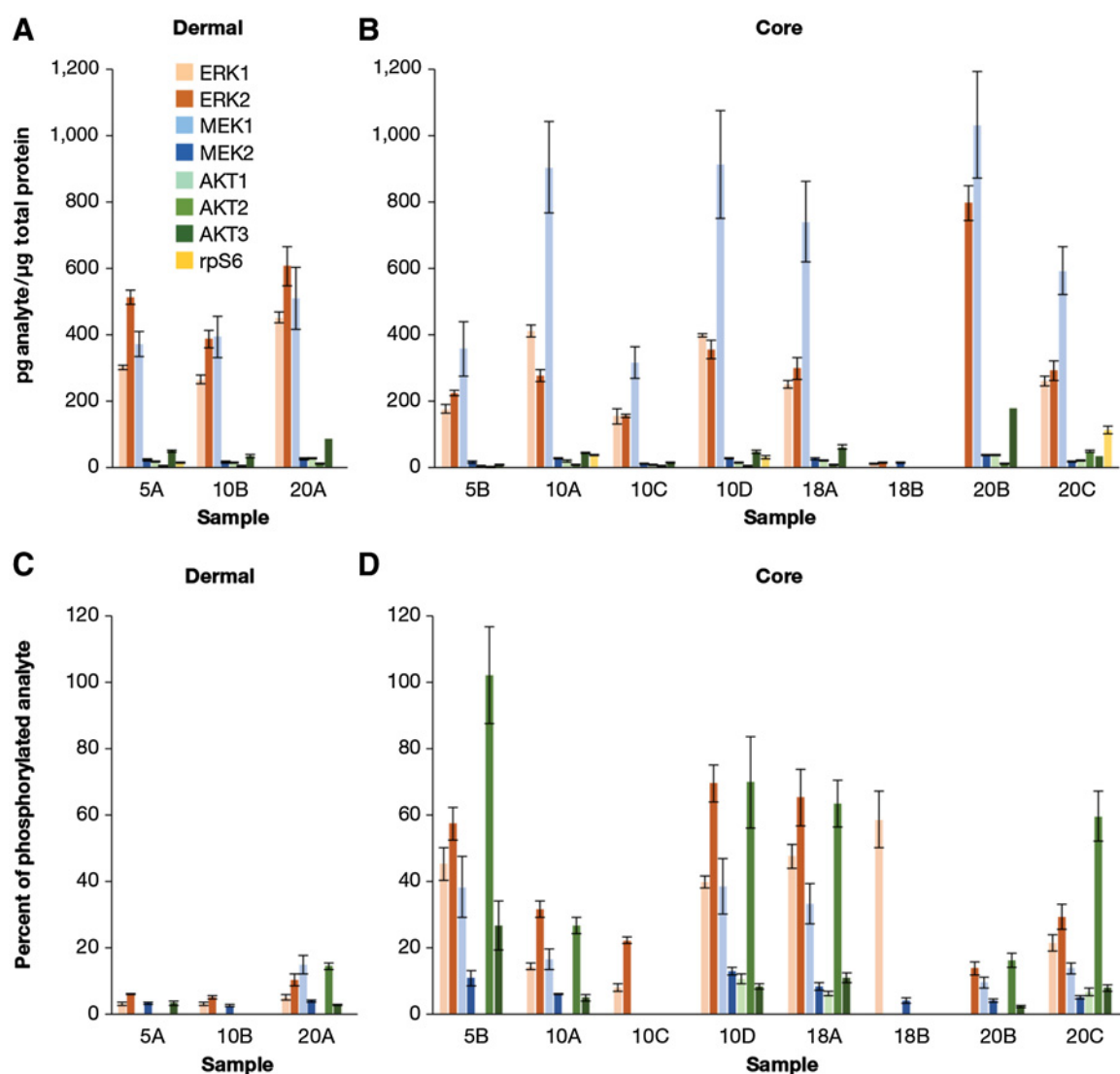
Figure 6.
Total protein levels and percent phosphorylation in biopsies from untreated patients with neurofibromas. Total protein levels are reported as picogram of analyte per microgram of total protein in dermal (**A**) and core needle (**B**) biopsies. Phosphorylation levels in dermal (**C**) and core needle (**D**) biopsies are reported as the percent of total analyte phosphorylated at sites assayed with this multiplex immunoassay. AKT samples refer to the Phospho A panel (Ser473/474/472-AKT1/2/3 and Ser235-rpS6). Patients are identified by number and distinct biopsy sites are lettered (e.g., 20A is from patient 20, biopsy site A). Error bars, SDs.

which often cross-react with other proteins and show high background noise in immunohistochemistry assays. AKT isoforms have redundant and nonredundant biological roles that have not yet been explored in a tumor tissue-specific manner before and after drug treatment. Our multiplex immunoassays allow us to discern the isoform ratios and determine if drug treatment alters the isoform composition as a result of feedback mechanisms. Our assays also include calibration materials, which allow quantifiable standardization of the reported values (as shown in **Fig. 6**) and a meaningful comparison of the results among patients within and across trials. Historical assays lack such calibration and rely on comparison of signal intensities in lysates before and after drug treatment. Even though a drug-induced percent change may be discerned if samples are analyzed strictly in a batched manner, signal readouts vary between experiments, making

comparison of biomarker levels from different batches error-prone. Furthermore, accurate measurement of biomarker changes requires the assay signals to be in the linear range of the assay, which is resolved by the use of standard curves. Finally, rigorous analytic validation of assays described in this study allows harmonization of pharmacodynamic data from different clinical trials versus assays where little is known about the specificity, accuracy, and sensitivity of the assays. We intend to make the assays described in this study available to clinical trial networks.

We have performed fit-for-purpose validation with three preclinical xenograft models of investigational cancer therapeutics, two PTEN-null models mimicking fitness for an ongoing clinical trial of the PI3Kβ inhibitor AZD8186 (NCT03218826) and one model from a previous trial that studied the AKT inhibitor MK-2206 and the MEK inhibitor

selumetinib (NCT01333475). As expected, given the PTEN-null status and the lack of activating mutations or overexpression in the MAPK pathway, AKT phosphorylation in HCC70 and PC3 xenografts was higher than in SW620 xenografts or patient neurofibroma biopsies. Consistent with a prior report describing the importance of AKT2 in PTEN-null tumor maintenance (17), AKT2 was also the most abundant and heavily phosphorylated isoform. Furthermore, treatment of HCC70 xenografts with AZD8186 potently inhibited Ser474-AKT2 phosphorylation after a single dose, and this inhibition was still observed in the first time point following 7 days of twice-daily treatment. Although PC3 xenografts also had high basal AKT2 phosphorylation and were maximally inhibited to a comparable degree, rebound levels of pAKT1/2 were elevated but only pSer474-AKT2 achieved statistical significance ($P = 0.045$ at 24 hours psd). Interestingly, despite similar degrees of maximal pAKT1/2 inhibition and greater inhibition of pSer235-rpS6 in HCC70, rpS6 phosphorylation rebounded more rapidly in HCC70 than in PC3. This could be attributed to differences in pharmacokinetics, that is, pAKT inhibition is greatest at 4 hours in PC3 versus 2 hours in HCC70, or to a greater abundance of pAKT3 (20). However, another intriguing possibility is that rpS6 is phosphorylated via MAPK pathway activity in HCC70 xenografts, which have significant increases in pThr202/Tyr204-ERK1 and pThr185/Tyr187-ERK2 phosphorylation at 7 hours psd ($P = 0.022$ and 0.0092, respectively, at 50 mg/kg). The lack of complete and durable pathway inhibition in these models is unsurprising, as prior studies reported only modest growth inhibition with AZD8186 monotherapy (40, 41). AZD8186-induced inhibition of pAKT (Ser473 and Thr308) in the HCC70 model reported here is comparable to results reported using a different assay platform (40); doses (50 mg/kg and 25 mg/kg) and time points (2, 4, and 24 hours) in our study were identical to this previous study to facilitate direct comparison. Overall, our data complement the results of these studies and support establishing a pharmacodynamics-guided dosing regimen that would achieve effective magnitude and duration of pathway suppression and accompanying tumor regression (24). However, this was beyond the scope of the current study. Furthermore, AZD8186 could possibly be more effective in combination with inhibitors that target adjacent (MAPK) or downstream (mTOR) pathways. We did not replicate a published efficacy study of AZD8186 (40) as identical doses in exact models were used in our pharmacodynamic studies and we expected similar results.

Although total levels of the AKT and MEK isoforms were relatively consistent between the different xenograft types, the PC3 and SW620 models had less of each ERK isoform than the HCC70 xenografts. However, as we would expect for a KRAS (G12V)-mutant cell line, SW620 xenografts had more pERK and pMEK (both in absolute terms and as a proportion of total analyte). SW620 xenografts also had approximately half the baseline rpS6 as the other models, but the ratio of phosphorylated to total rpS6 was similar in all models. Treatment of SW620 xenografts with a single dose of selumetinib induced near-complete reductions of pThr202/Tyr204-ERK1 and pThr185/Tyr187-ERK2, respectively, for at least 4 hours, but phosphorylation returned to vehicle levels by 24 hours; duration was not improved with 3 weeks of treatment. Also, a single dose of selumetinib induced hyperphosphorylation of both pThr305-AKT3 and pSer472-AKT3 at 24 hours psd and a corresponding increase in rpS6 phosphorylation at both pSer235-rpS6 at 24 hours psd and pSer240/244-rpS6 at 48 hours psd. Reductions of pSer235-rpS6 and pSer240/244-rpS6 were significant at early time points and greatest with the com-

bination therapy, supporting the concept that multipathway targeting may be essential for treating this type of cancer. However, this combination was dose-limited by toxicity, resulting in lower than effective doses for selumetinib, limited efficacy in preclinical study, and failure to achieve the endpoint goal of at least 70% pERK inhibition post-treatment in a phase II trial (42). Pharmacokinetic–pharmacodynamic relationships of multiple MEK inhibitors have been examined in mouse models (43–45); tumor regressions were reported with sustained pERK1/2 inhibition (70%–80% for 7–8 hours). Therefore, pharmacokinetic measurements were redundant in our study because a pharmacodynamic measurement alone is sufficient to demonstrate target engagement consistent with predicted pharmacokinetic–pharmacodynamic modeling. Our pharmacodynamic results in the SW620 model (**Fig. 5**) are consistent with published pharmacokinetic results with a 25 mg/kg selumetinib dose (44) and confirm that twice-daily dosing is needed to sustain the >80% pERK inhibition.

To verify the utility of this assay in clinical trial samples, untreated neurofibroma tissue biopsies were analyzed from NF1 patients with plexiform neurofibromas (NCT02407405). These included three cNF dermal shave biopsies because they were less invasive than needle core biopsies, but protein extraction proved to be challenging due to the physical characteristics of the samples. Despite these challenges, MEK/ERK levels were measured in nearly all untreated samples at concentrations sufficient to measure up to 90% inhibition if compared with treated biopsies. Total AKT1/2/3 was measured in all but one sample, however rpS6 and pAKT levels were low in most samples. Because of the limited number of samples, our data do not fully disclose whether dermal biopsies can provide a less invasive option of sampling, but the results do demonstrate that the assays are fit-for-purpose for clinical evaluation of the agents of interest. The utility of these multiplexed measurements lies in identifying basal level of activation of the PI3K/AKT and MEK/ERK pathways and the level of activation of PI3K/AKT in response to treatment as a potential mechanism of resistance.

Authors' Disclosures

R.E. Parchment reported other from NIH/NCI during the conduct of the study. No potential conflicts of interest were disclosed by the other authors.

Disclaimer

The content of this publication does not necessarily reflect the views or policies of the Department of Health and Human Services, nor does mention of trade names, commercial products, or organizations imply endorsement by the U.S. Government.

Authors' Contributions

W.G. Herrick: Conceptualization, formal analysis, validation, investigation, methodology, writing–original draft, writing–review and editing. **C.L. Kilpatrick:** Conceptualization, formal analysis, validation, investigation, methodology, writing–review and editing. **M.G. Hollingshead:** Conceptualization, formal analysis, supervision, funding acquisition, methodology, writing–review and editing. **D. Esposito:** Formal analysis, investigation, methodology, writing–review and editing. **G. O'Sullivan Coyne:** Conceptualization, formal analysis, investigation, writing–review and editing. **A.M. Gross:** Formal analysis, writing–review and editing. **B.C. Johnson:** Formal analysis, writing–original draft, writing–review and editing. **A.P. Chen:** Conceptualization, supervision, project administration, writing–review and editing. **B.C. Widemann:** Conceptualization, supervision, project administration, writing–review and editing. **J.H. Doroshow:** Conceptualization, supervision, funding acquisition, project administration, writing–review and editing. **R.E. Parchment:** Conceptualization, supervision, funding acquisition,

References

1. Lawrence MS, Stojanov P, Mermel CH, Robinson JT, Garraway LA, Golub TR, et al. Discovery and saturation analysis of cancer genes across 21 tumour types. Nature 2014;505:495–501.
2. Steelman LS, Pohnert SC, Shelton JG, Franklin RA, Bertrand FE, McCubrey JA. JAK/STAT, Raf/MEK/ERK, PI3K/Akt and BCR-ABL in cell cycle progression and leukemogenesis. Leukemia 2004;18:189–218.
3. Degirmenci U, Wang M, Hu J. Targeting aberrant RAS/RAF/MEK/ERK signaling for cancer therapy. Cells 2020;9:198.
4. Shariati M, Meric-Bernstam F. Targeting AKT for cancer therapy. Expert Opin Investig Drugs 2019;28:977–88.
5. Borson-Chazot F, Dantony E, Illouz F, Lopez J, Niccoli P, Wassermann J, et al. Effect of buparlisib, a pan-class I PI3K inhibitor, in refractory follicular and poorly differentiated thyroid cancer. Thyroid 2018;28:1174–9.
6. Edelman G, Rodon J, Lager J, Castell C, Jiang J, Van Allen EM, et al. Phase I trial of a tablet formulation of pilaralisib, a pan-class I PI3K inhibitor, in patients with advanced solid tumors. Oncologist 2018;23:401–e38.
7. Juric D, Castel P, Griffith M, Griffith OL, Won HH, Ellis H, et al. Convergent loss of PTEN leads to clinical resistance to a PI(3)Kalpha inhibitor. Nature 2015;518:240–4.
8. Renshaw J, Taylor KR, Bishop R, Valenti M, De Haven Brandon A, Gowan S, et al. Dual blockade of the PI3K/AKT/mTOR (AZD8055) and RAS/MEK/ERK (AZD6244) pathways synergistically inhibits rhabdomyosarcoma cell growth in vitro and in vivo. Clin Cancer Res 2013;19:5940–51.
9. Ryan MB, Fece de la Cruz F, Phat S, Myers DT, Wong E, Shahzade HA, et al. Vertical pathway inhibition overcomes adaptive feedback resistance to KRASG12C inhibition. Clin Cancer Res 2020;26:1633–43.
10. Merchant M, Moffat J, Schaefer G, Chan J, Wang X, Orr C, et al. Combined MEK and ERK inhibition overcomes therapy-mediated pathway reactivation in RAS mutant tumors. PLoS One 2017;12:e0185862.
11. Wang H, Huang F, Zhang Z, Wang P, Luo Y, Li H, et al. Feedback activation of SGK3 and AKT contributes to rapamycin resistance by reactivating mTORC1/4EBP1 axis via TSC2 in breast cancer. Int J Biol Sci 2019;15:929–41.
12. Meng S, Wang G, Lu Y, Fan Z. Functional cooperation between HIF-1alpha and c-Jun in mediating primary and acquired resistance to gefitinib in NSCLC cells with activating mutation of EGFR. Lung Cancer 2018;121:82–90.
13. Bago R, Sommer E, Castel P, Crafter C, Bailey FP, Shpiro N, et al. The hVps34-SGK3 pathway alleviates sustained PI3K/Akt inhibition by stimulating mTORC1 and tumour growth. EMBO J 2016;35:1902–22.
14. Flaherty KT, Robert C, Hersey P, Nathan P, Garbe C, Milhem M, et al. Improved survival with MEK inhibition in BRAF-mutated melanoma. N Engl J Med 2012;367:107–14.
15. Ferry-Galow KV, Makhlouf HR, Wilsker DF, Lawrence SM, Pfister TD, Marrero AM, et al. The root causes of pharmacodynamic assay failure. Semin Oncol 2016;43:484–91.
16. Ragon BK, Odenike O, Baer MR, Stock W, Borthakur G, Patel K, et al. Oral MEK 1/2 inhibitor trametinib in combination with AKT inhibitor GSK2141795 in patients with acute myeloid leukemia with RAS mutations: a phase II study. Clin Lymphoma Myeloma Leuk 2019;19:431–40.
17. Chin YR, Yuan X, Balk SP, Toker A. PTEN-deficient tumors depend on AKT2 for maintenance and survival. Cancer Discov 2014;4:942–55.
18. Ercan D, Xu C, Yanagita M, Monast CS, Pratilas CA, Montero J, et al. Reactivation of ERK signaling causes resistance to EGFR kinase inhibitors. Cancer Discov 2012;2:934–47.
19. Kong X, Kuilman T, Shahrabi A, Boshuizen J, Kemper K, Song JY, et al. Cancer drug addiction is relayed by an ERK2-dependent phenotype switch. Nature 2017;550:270–4.
20. Nakatani K, Thompson DA, Barthel A, Sakaue H, Liu W, Weigel RJ, et al. Up-regulation of Akt3 in estrogen receptor-deficient breast cancers and androgen-independent prostate cancer lines. J Biol Chem 1999;274:21528–32.
21. Park ER, Eblen ST, Catling AD. MEK1 activation by PAK: a novel mechanism. Cell Signal 2007;19:1488–96.
22. Liu X, Xu Y, Zhou Q, Chen M, Zhang Y, Liang H, et al. PI3K in cancer: its structure, activation modes and role in shaping tumor microenvironment. Future Oncol 2018;14:665–74.
23. de Graaf EL, Kaplon J, Mohammed S, Vereijken LA, Duarte DP, Redondo Gallego L, et al. Signal transduction reaction monitoring deciphers site-specific PI3K-mTOR/MAPK pathway dynamics in oncogene-induced senescence. J Proteome Res 2015;14:2906–14.
24. Srivastava AK, Hollingshead MG, Govindharajulu JP, Covey JM, Liston D, Simpson MA, et al. Molecular pharmacodynamics-guided scheduling of biologically effective doses: a drug development paradigm applied to MET tyrosine kinase inhibitors. Mol Cancer Ther 2018;17:698–709.
25. Teicher BA. Anticancer drug development guide: preclinical screening, clinical trials, and approval. Totowa, N.J.: Humana Press; 1997.xii, 311 p.
26. Barlaam B, Cosulich S, Degorce S, Fitzek M, Green S, Hancox U, et al. Discovery of (R)-8-(1-(3,5-difluorophenylamino)ethyl)-N,N-dimethyl-2-morpholino-4-oxo-4H-chrom ene-6-carboxamide (AZD8186): a potent and selective inhibitor of PI3Kbeta and PI3Kdelta for the treatment of PTEN-deficient cancers. J Med Chem 2015;58:943–62.
27. Hirai H, Sootome H, Nakatsuru Y, Miyama K, Taguchi S, Tsujioka K, et al. MK-2206, an allosteric Akt inhibitor, enhances antitumor efficacy by standard chemotherapeutic agents or molecular targeted drugs in vitro and in vivo. Mol Cancer Ther 2010;9:1956–67.
28. Srivastava AK, Hollingshead MG, Weiner J, Navas T, Evrard YA, Khin SA, et al. Pharmacodynamic response of the MET/HGF receptor to small-molecule tyrosine kinase inhibitors examined with validated, fit-for-clinic immunoassays. Clin Cancer Res 2016;22:3683–94.
29. Kaufmann D. Neurofibromatoses. New York, NY:Karger; 2008. p. 192.
30. National Institutes of Health Consensus Development Conference Statement: neurofibromatosis. Bethesda, MD, USA, July 13–15, 1987. Neurofibromatosis 1988;1:172–8.
31. Ferner RE, Gutmann DH. Neurofibromatosis type 1 (NF1): diagnosis and management. Handb Clin Neurol 2013;115:939–55.
32. Liu J, Weiss HL, Rychahou P, Jackson LN, Evers BM, Gao T. Loss of PHLPP expression in colon cancer: role in proliferation and tumorigenesis. Oncogene 2009;28:994–1004.
33. Marques RB, Aghai A, de Ridder CMA, Stuurman D, Hoeben S, Boer A, et al. High efficacy of combination therapy using PI3K/AKT inhibitors with androgen deprivation in prostate cancer preclinical models. Eur Urol 2015;67:1177–85.
34. Cherrin C, Haskell K, Howell B, Jones R, Leander K, Robinson R, et al. An allosteric Akt inhibitor effectively blocks Akt signaling and tumor growth with only transient effects on glucose and insulin levels in vivo. Cancer Biol Ther 2010;9:493–503.
35. Emery CM, Vijayendran KG, Zipser MC, Sawyer AM, Niu L, Kim JJ, et al. MEK1 mutations confer resistance to MEK and B-RAF inhibition. Proc Natl Acad Sci U S A 2009;106:20411–6.
36. VanderLaan PA. Fine-needle aspiration and core needle biopsy: an update on 2 common minimally invasive tissue sampling modalities. Cancer Cytopathol 2016;124:862–70.
37. Bessadottir M, Skuladottir EA, Gowan S, Eccles S, Ogmundsdottir S, Ogmundsdottir HM. Effects of anti-proliferative lichen metabolite, protolichesterinic acid on fatty acid synthase, cell signalling and drug response in breast cancer cells. Phytomedicine 2014;21:1717–24.

38. Gowan SM, Hardcastle A, Hallsworth AE, Valenti MR, Hunter LJ, de Haven Brandon AK, et al. Application of meso scale technology for the measurement of phosphoproteins in human tumor xenografts. Assay Drug Dev Technol 2007;5: 391–401.

39. Smolko CM, Janes KA. An ultrasensitive fiveplex activity assay for cellular kinases. Sci Rep 2019;9:19409.

40. Hancox U, Cosulich S, Hanson L, Trigwell C, Lenaghan C, Ellston R, et al. Inhibition of PI3Kbeta signaling with AZD8186 inhibits growth of PTEN-deficient breast and prostate tumors alone and in combination with docetaxel. Mol Cancer Ther 2015;14:48–58.

41. Lynch JT, Polanska UM, Hancox U, Delpuech O, Maynard J, Trigwell C, et al. combined inhibition of PI3Kbeta and mTOR inhibits growth of PTEN-null tumors. Mol Cancer Ther 2018;17:2309–19.

42. Do K, Speranza G, Bishop R, Khin S, Rubinstein L, Kinders RJ, et al. Biomarker-driven phase 2 study of MK-2206 and selumetinib (AZD6244,

ARRY-142886) in patients with colorectal cancer. Invest New Drugs 2015;33: 720–8.

43. Daouti S, Higgins B, Kolinsky K, Packman K, Wang H, Rizzo C, et al. Preclinical in vivo evaluation of efficacy, pharmacokinetics, and pharmacodynamics of a novel MEK1/2 kinase inhibitor RO5068760 in multiple tumor models. Mol Cancer Ther 2010;9:134–44.

44. Davies BR, Logie A, McKay JS, Martin P, Steele S, Jenkins R, et al. AZD6244 (ARRY-142886), a potent inhibitor of mitogen-activated protein kinase/extra-cellular signal-regulated kinase kinase 1/2 kinases: mechanism of action in vivo, pharmacokinetic/pharmacodynamic relationship, and potential for combination in preclinical models. Mol Cancer Ther 2007;6:2209–19.

45. Wong H, Vernillet L, Peterson A, Ware JA, Lee L, Martini JF, et al. Bridging the gap between preclinical and clinical studies using pharmacokinetic-pharmacodynamic modeling: an analysis of GDC-0973, a MEK inhibitor. Clin Cancer Res 2012;18:3090–9.